Nuclear Instruments and Methods in Physics Research A 1072 (2025) 170195

Contents lists available at ScienceDirect

Nuclear Inst. and Methods in Physics Research, A

journal homepage: www.elsevier.com/locate/nima

Full Length Article

Active harmonic EU cavity: Commissioning and operation with beam ☆,☆☆

F. Perez [a,*], J. Alvarez [a], I. Bellafont [a], B. Bravo [a], J. Ocampo [a], A. Salom [a], P. Solans [a], M. Ebert [b], N.-O. Fröhlich [b], P. Hülsmann [b], R. Onken [b], W. Anders [c], V. Duerr [c], T. Löwner [c], A. Matveenko [c], M. Ries [c], L. Shi [c], Y. Tamashevich [c], A. Tsakanian [c], H. De Gersem [d], W. Müller [d]

[a] ALBA Synchrotron - CELLS, C/Llum 2-26, Cerdanyola del Vallès, 08290, Barcelona, Spain
[b] Deutsches Elektronen-Synchrotron (DESY), Noktstrasse 85, 22607 Hamburg, Germany
[c] Helmholtz-Zentrum Berlin (HZB), Hahn-Meitner-Platz 1, 14109, Berlin, Germany
[d] Institute for Accelerator Science and Electromagnetic Fields (TEMF), Schloßgartenstr. 8, 64289 Darmstadt, Germany

ARTICLE INFO

Keywords:
Radiofrequency
Active 3rd harmonic cavity
Digital LLRF
Longitudinal beam dynamics

ABSTRACT

ALBA is a 3rd generation synchrotron light source located in Spain, in operation since 2012. In preparation for its upgrade to a 4th generation facility, which requires addressing the significantly reduced Touschek lifetime, ALBA has designed and constructed a higher-order mode (HOM) damped active 3rd harmonic RF cavity. This cavity is designed to longitudinally lengthen the electron bunches, thereby reducing their density and enhancing the beam lifetime. The design is based on the EU HOM-damped cavity currently employed in ALBA's main radio frequency (RF) system. The cavity prototype was installed in the BESSY II ring under a collaborative agreement between ALBA, HZB, and DESY, institutions that operate at the same main RF frequency, 500 MHz. This paper presents the first commissioning results, including bead-pull measurements, high-power conditioning and initial beam tests in both single and multi-bunch operation modes. The results confirm that the cavity parameters are consistent with the design specifications, the HOMs are effectively mitigated, and the anticipated beam lifetime enhancement is achieved, demonstrating the feasibility of the designed cavity.

1. Introduction

Many synchrotron light sources are currently transitioning from the third to the fourth generation [1–7]. A key challenge in these upgrades is maintaining a reasonable beam lifetime despite the significant reduction in transverse emittance. Harmonic radio frequency (RF) systems are widely employed to mitigate beam lifetime reduction caused by the low emittance and the associated increase in the Touschek scattering effect. The addition of the harmonic system provides longitudinal bunch lengthening, reducing the electron density and enhancing the Touschek lifetime.

While active harmonic cavities have been utilized historically (e.g., NSLS-VUV [8]), most modern light sources, such as MAX IV [9], ALS [10], BESSY II [11], Elettra, and SLS [12] rely on passive cavities. Passive cavities, whether normal-conducting or superconducting, operate using beam-induced voltage, which is regulated through resonance frequency tuning. Since in passive cavities the synchronous phase is inherently tied to the resonance frequency, it is not possible to achieve the optimal phase across the entire beam current range. Additionally, in case of normal conducting ones, their low shunt impedance restricts their operation primarily to high beam currents. Although superconducting passive harmonic cavities, such as those used at Elettra [12], offer superior power efficiency, support operation at low beam currents, and enable higher voltages per cavity unit, their higher cost and operational complexity make them less suitable for most synchrotron light facilities, particularly those lacking the existing infrastructure to support superconducting RF technology.

Normal conducting active harmonic systems, though more complex and costly than normal conducting passive ones, offer several advantages: (i) They enable optimal bunch lengthening across the entire

☆ The cavity prototype design and construction were co-funded by the European Regional Development Fund (ERDF) within the Framework of the Smart Growth Operative Programme 2014-2020.
☆☆ This work has been performed under the Collaboration Agreement RCN-CIN202100124, Spanish BOE Resolution 8506 of May 14th, 2021, published in May 21st, 2021.
* Corresponding author.
E-mail address: francis@cells.es (F. Perez).

https://doi.org/10.1016/j.nima.2024.170195
Received 31 October 2024; Received in revised form 24 December 2024; Accepted 28 December 2024
Available online 6 January 2025

beam current range, with significant benefits for single-bunch operation. Machine studies conducted in low-current, single-bunch mode provide valuable insights into RF system dynamics. (ii) Active systems deliver more stable cavity fields through low-level RF (LLRF) control, enhancing thermal stability and eliminating issues such as plunger movement. (iii) They support advanced feedforward and feedback mechanisms, which help mitigate instabilities and compensate for transient beam loading [13,14].

ALBA, a 3rd generation synchrotron light source located in Spain, has been in operation since 2012 and is now preparing for its 4th generation upgrade [1]. To address the significant reduction in Touschek lifetime of its upgrade, ALBA designed and constructed a prototype of a 1.5 GHz, active, normal-conducting, higher-order mode (HOM) damped, 3rd harmonic cavity [15]. The cavity, known as 3rd Harmonic EU cavity, is based on the 500 MHz EU HOM-damped cavity design [16,17] currently employed in ALBA's main RF system.

To validate the cavity design and performance, ALBA initiated a collaboration with HZB and DESY, two German institutions that, like ALBA, are transitioning their synchrotron light sources from the third to the fourth generation [4,5]. All three institutions share the same main RF frequency of 500 MHz, meaning their harmonic cavities operate at 1.5 GHz. Through this collaborative agreement, the cavity prototype was tested in the BESSY II ring at HZB, benefiting all parties by providing an harmonic cavity design adaptable to their specific upgrade requirements.

This paper presents the first commissioning results from the 3rd Harmonic EU Cavity, operating in active mode. The cavity is powered by an RF amplifier and controlled via digital LLRF, allowing full control of harmonic voltage amplitude and phase for any beam current. Section 2 provides a brief overview of the double RF system theory. Section 3 summarizes the design, construction, and testing of the prototype cavity. Section 4 presents tests with beam results, including single and multi-bunch operation modes.

2. Double RF system theory

In a double RF system the total accelerating voltage seen by a particle on every turn is given by the sum of the cavity voltages and their relative phase to the beam:

$$V_t(\phi) = V_{mc}\ \sin(\phi_s + \phi) + V_{hc}\ \sin(\phi_h + n\phi) \tag{1}$$

where V_{mc} and V_{hc} are the voltage amplitudes of the main and harmonic cavities, respectively, the terms ϕ_s and ϕ_h represent the synchronous phases for the main and harmonic systems, ϕ is the particle's phase offset with respect to the main synchronous phase, and n is the harmonic order.

When the harmonic phase and voltage are set such that both the first and second derivatives of the total voltage are zero at the synchronous phase, a quartic potential well is created, resulting in the so-called flat potential condition. This flatter potential reduces the oscillation speed of particles within their bucket, leading to longer bunch lengths, lower peak charge densities, and an extended beam lifetime, without altering the beam energy distribution. The reduced peak charge density and increased bunch length also mitigate the intrabeam scattering effect, which otherwise contributes to emittance growth. Furthermore, operation near the flat potential condition enhances Landau damping, driven by the broader distribution of synchrotron frequencies.

The conditions to achieve flat potential are [18]:

$$V_{hc,fp} = V_{mc}\sqrt{\frac{1}{n^2} - \frac{1}{n^2-1}\left(\frac{U_0}{e_0 V_{mc}}\right)^2} \tag{2}$$

$$tan\,\phi_{h,fp} = -\frac{nU_0}{e_0 V_{mc}}\frac{1}{\sqrt{(n^2-1)^2 - n^4\left(\frac{U_0}{e_0 V_{mc}}\right)^2}} \tag{3}$$

where U_0 represents the energy loss per turn due to synchrotron radiation, e_0 denotes the elementary charge, and the subscript fp refers to the flat potential case.

The negative of the ratio of the longitudinal restoring force of the harmonic system with respect to that of the fundamental one is represented by ξ, defined in [19,20] but adapted here to the sine convention of the synchronous phase for the sake of consistency:

$$\xi = \frac{-nV_{hc}\cos\phi_h}{V_{mc}\cos\phi_s} \tag{4}$$

For $0 < \xi < 1$, the synchrotron frequency is reduced and the bunches are lengthened. $\xi = 1$ corresponds to the flat potential case, when the forces of the main and harmonic system cancel each other and there is no net linear restoring force, and thus the linear synchrotron frequency of the synchronous particle is zero [19]. Significant bunch lengthening occurs above 0.9, but depending on the system's parameters beam instabilities ascribed to the double RF system may arise well before reaching flat potential, around values >0.95 [20,21]. When $\xi > 1$, the synchroton potential becomes a double well with two minima, which results in a double-hump longitudinal bunch shape, often unstable and not desired for operation. ξ is thus an useful figure to assess the system's closeness to what we consider the case of optimal bunch lengthening, $\xi = 1$.

3. Harmonic EU cavity

3.1. Design and key features

The 3rd Harmonic EU cavity adopts a pillbox design with nose cones, providing a maximum accelerating voltage of 200 kV at 1.5 GHz. The diameter of the cavity body is 136.9 mm and the length between end walls is 104 mm. The cavity is 300 mm long from flange to flange. It is intended to be used as an active third harmonic RF cavity for synchrotron light sources. A cavity prototype was manufactured during 2020–2021 in collaboration between AVS Added Value Solutions (Spain) and VITZRO NEXTECH (South Korea) [22].

Fig. 1 provides a render image highlighting the main cavity components and a picture of the prototype taken during the site acceptance tests:

Fig. 2 shows the electromagnetic model of the prototype cavity. Three circular ridged waveguides extract HOMs from the cavity body, with a cutoff frequency of 1.72 GHz to avoid damping the fundamental mode. In earlier designs, in-vacuum ferrites were placed at the ends of these waveguides to dissipate HOMs power. As an advancement over previous designs, this cavity replaces the ferrites with transitions to coaxial N-type connectors, termed "transdampers". The transdampers redirect HOMs power to external RF loads, eliminating the need for in-vacuum ferrites. This design simplifies manufacturing and enables direct HOMs monitoring via external devices [23].

As seen in 3, each transdamper consists of two sections: a transition from a circular ridged waveguide to a rectangular waveguide, and a broadband transition from the rectangular waveguide to a coaxial connector [15]. Vacuum isolation is achieved using a commercial broadband coaxial vacuum feedthrough. The transdampers efficiently couple frequencies between 1.75 GHz and 5.3 GHz, converting circular TE_{11} modes into coaxial TEM modes in a two-step process. First, the ridged circular waveguide TE_{11}-like mode is transformed into a rectangular TE_{10} mode. Subsequently, this rectangular mode is converted into a coaxial TEM mode via a rectangular waveguide-to-N-coaxial transition.

Using the frequency domain solver in CST Microwave Studio [24], the simulated transmission (S_{21}) and reflection (S_{11}) coefficients of the ridged circular TE_{11} mode were calculated across the 1.75 GHz to 6 GHz frequency range, to safely cover both the beam pipe cutoff frequency of 3.8 GHz and the maximum design frequency of the Transdampers of 5 GHz. The results are presented in Fig. 4.

RF power is delivered to the cavity via an EIA 3-1/8 coaxial line. An electromagnetic model of this coupler is presented in Fig. 5. Two

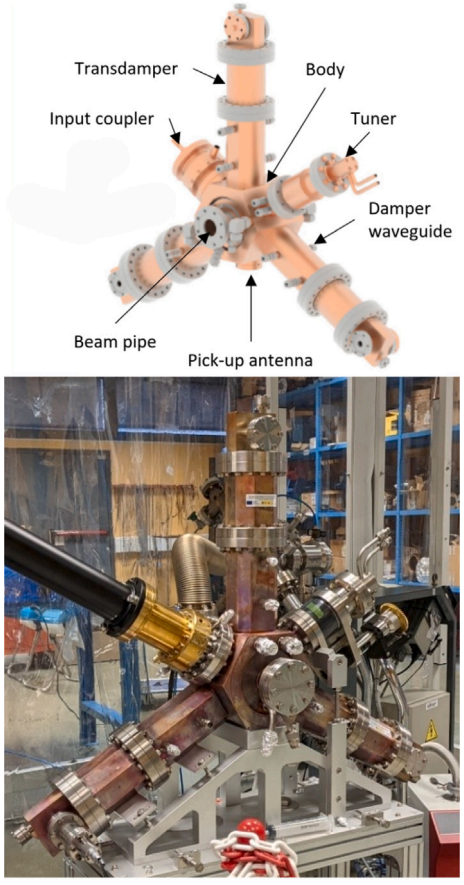

Fig. 1. Top: Representation of Harmonic EU cavity components. Bottom: Harmonic EU cavity prototype during the site acceptance test.

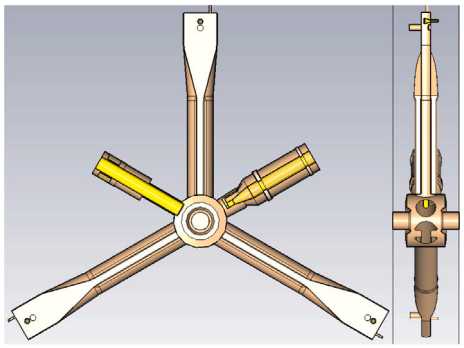

Fig. 2. Electromagnetic model of the cavity prototype, showing frontal and lateral section views.

alumina disks hold the inner conductor in place and provide vacuum isolation. An inductive loop at the end of the coaxial line couples the power to the cavity body. The coupler allows the adjustment of the coupling factor (β) by rotating the waveguide along the central axis. This rotation changes the angle of the coupling loop with respect to the magnetic field of the TM010 accelerating mode.

The cavity also features a 35 mm diameter cylindrical plunger that allows fine-tuning of the resonant frequency by moving in and out of the cavity.

Table 1
Measured tuning range of the cavity prototype.

Parameter	Frequency [GHz]	Plunger position [mm]
Maximum frequency	1.5041	44
Central frequency	1.4979	31
Minimum frequency	1.4917	0
Total tuning range	12.4	–

Table 2
Main cavity parameters measured at the central resonance frequency, f_0.

Parameter	Symbol	Value	Unit
Reflection coefficient	S_{11}	−50.8	dB
Coupling factor	β	1.006	–
Bandwidth	BW	214	kHz
Loaded quality factor	Q_l	6995	–
Unloaded quality factor	Q_0	14 031	–
Transmission to pick-up antenna	S_{21}	−45.9	dB

3.2. Low RF power measurements

Upon reception of the cavity prototype, some low power RF measurements were made to validate the performance of the manufactured cavity. Table 1 presents the frequency range achievable by the cavity prototype when the plunger is moved across its full range. The measured tuning range of 12.4 MHz allows the cavity to be detuned by several revolution frequencies when installed in the BESSY II storage ring.

Fig. 6 illustrates the variation in the resonant frequency and quality factor as the plunger position changes over the entire tuning range.

At the central frequency of 1.4979 GHz measured in Table 1, the input coupler angle was adjusted to minimize reflected power, achieving critical coupling ($\beta = 1$). Table 2 summarizes the key low-power measurements obtained under this condition.

Additionally, the ability of the transdampers to couple into the cavity body was assessed by measuring the RF transmission between two transdampers using a Vector Network Analyzer (VNA). Fig. 7 shows the transmission measurement, where the predicted 1.7 GHz cutoff frequency of the damper arms is evident. The observed signal transmission between the two arms, mediated by the cavity body, confirms the capability of the transdampers to effectively couple HOMs within the cavity.

The cavity's vacuum quality was tested by pumping its volume with a turbo-molecular pump. After 72 h of pumping, the pressure dropped to 3×10^{-7} mbar. No leaks were detected. Residual Gas Analyzer (RGA) analysis indicated that hydrocarbon contamination was approximately three orders of magnitude below the partial pressure of water vapor.

3.3. HOM analysis

The HOM analysis of the 3rd harmonic RF cavity was conducted using eigenmode simulations in CST Microwave Studio [24] for the first 300 modes and up to the TM_{01}-mode cutoff frequency of the beam pipe, ≈5.0 GHz. The first mode corresponds to the fundamental frequency, while the remaining 299 modes are HOMs. The simulations were performed on a tetrahedral mesh with curved elements of second order to allow for a good approximation of the cylindrical walls of the cavity and the HOM dampers. The eigenmodes on this grid were calculated with second order of the eigenmode solver to reach accurate results within reasonable time. The computational domain is enclosed by the metallic walls of the cavity. The only openings are the input coupler and the three HOM couplers, which are considered as ports, and the beam pipes, which were closed by metallic walls in sufficiently large distance. The first 300 modes means This allowed the impedance spectra for the cavities to be derived and compared to the calculated longitudinal and transverse instability thresholds, $Z_{\parallel}^{thresh}$ and $Z_{\perp}^{thresh}$, respectively. Fig. 8 illustrates the longitudinal shunt impedances of

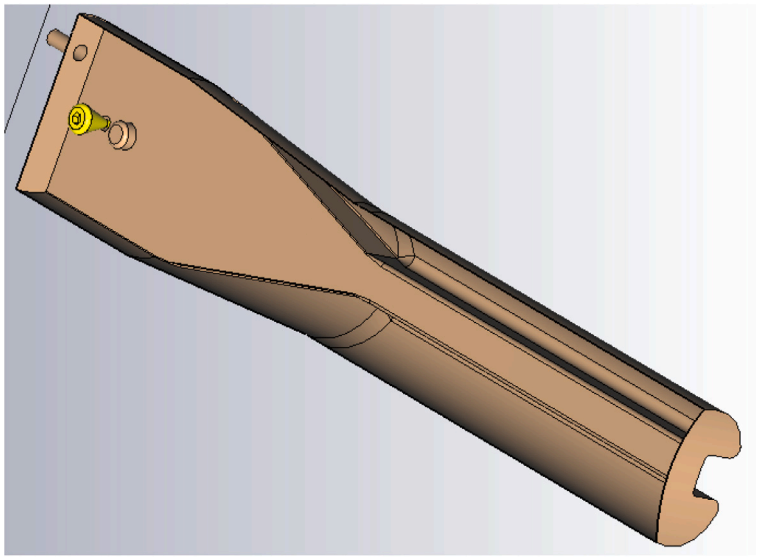

Fig. 3. Electromagnetic model of a transdamper.

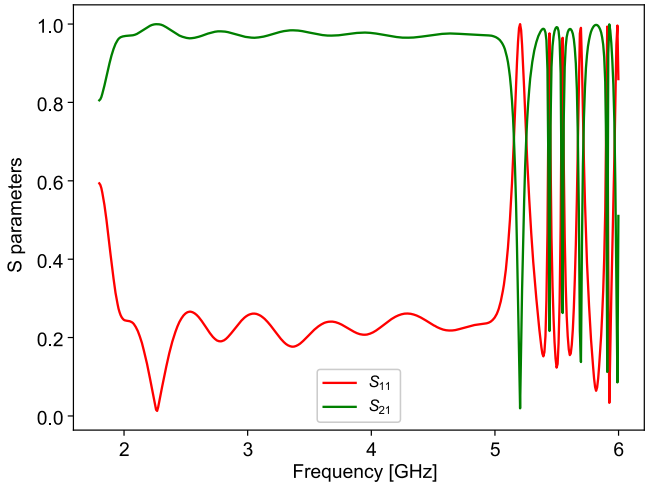

Fig. 4. S_{11} and S_{21} of the transdamper from 1.75 to 6 GHz simulated with CST MWS Studio.

Table 3
Input data used to calculate the impedance budgets of BESSY II.

Parameter	Symbol	Value	Unit
Revolution frequency	f_{rev}	1.2492	MHz
Beam current	I_b	300	mA
Beam energy	E	1.7	GeV
Momentum compaction factor	α	$7.3 \cdot 10^{-4}$	–
Synchrotron frequency	f_s	$7.0 \cdot 10^{3}$	Hz
Beta function	β	5.0	m
Longitudinal damping decrement	τ_s	752	s^{-1}
Transversal damping decrement	$\tau_{x,y}$	250	s^{-1}

Table 4
HOM external quality factor and R/Q ratio. The shunt impedance, R, follows the convention $P = \frac{V^2}{2R}$, where P is the power dissipated in the cavity and V the cavity voltage.

Frequency [GHz]	External Q	R/Q [Ω]
1.821	101.14	14.48
1.905	97.89	9.85
1.994	23.58	0.29
2.105	68.00	47.32
2.198	20.03	0.02

the first 300 HOMs, including the fundamental mode. The blue curve represents the longitudinal impedance threshold for BESSY II, above which coupled-bunch instabilities may occur. As expected, the shunt impedance of the fundamental mode exceeds the instability threshold, while the remaining 299 modes remain well below it. Fig. 9 shows the transverse shunt impedances for the simulated modes, excluding the fundamental mode, which intrinsically has no transverse effect. The plot confirms that all transverse shunt impedances are significantly below the instability threshold. The thresholds were calculated using Eqs. (5) and (6), using input data from Table 3:

$$Z_{\parallel}^{thresh}(f) = \frac{\tau_s}{f} \frac{2E f_s}{I_b \alpha f_{rev}}, \tag{5}$$

$$Z_{\perp}^{thresh}(f) = \frac{\tau_{x,y}}{f_{rev}} \frac{2E}{I_b \beta}, \tag{6}$$

Among the 300 modes analyzed, only one mode, at 2.105 GHz, interacts significantly with the beam. This mode exhibits an external quality factor of 68, indicating sufficient damping to prevent adverse effects on the particle beam. However, substantial RF power couples to this mode and propagates through the higher-order mode couplers and the hollow waveguide-to-coaxial transition. Additionally, four higher-order modes exhibit weak coupling to the beam at 1.821, 1.905, 1.994, and 2.198 GHz, respectively. As shown in Table 4, all of these modes have external quality factors below 100, ensuring effective coupling to the HOM dampers and sufficient damping.

Determining the longitudinal and transverse shunt impedances of the HOMs in this type of HOM-damped cavity presents significant challenges, ascribed to the unique characteristics of the cavity design and the presence of HOM couplers with large coupling apertures attached to the cavity body. In the presented cavity, the following phenomena are observed:

- *Mode distortion:* With the exception of the fundamental mode, all higher-order modes are significantly perturbed, losing their distinct classification as pure TM- or TE-type modes. Instead, hybrid modes, referred to as HEM (Hybrid Electromagnetic) modes, are observed.
- *Misalignment of axes:* The electrical axis of the cavity no longer aligns with the beam axis, and in some cases, it is skewed relative to the beam axis. This misalignment arises primarily due to the asymmetric longitudinal distribution of the three HOM couplers,

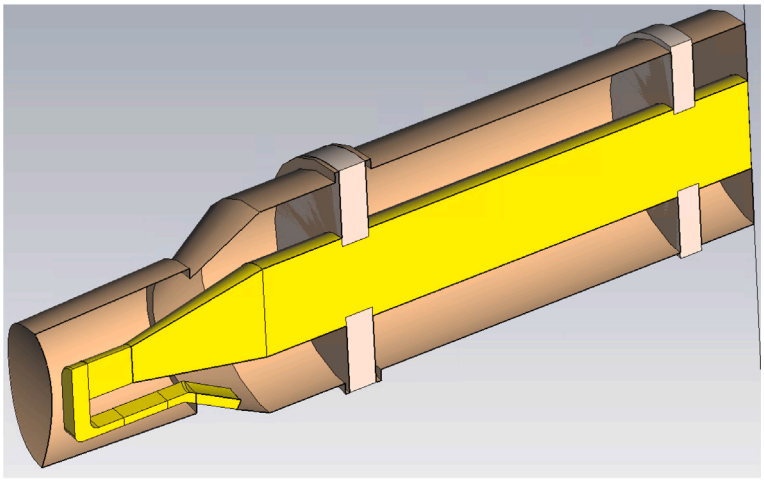

Fig. 5. Electromagnetic model of the RF input coupler.

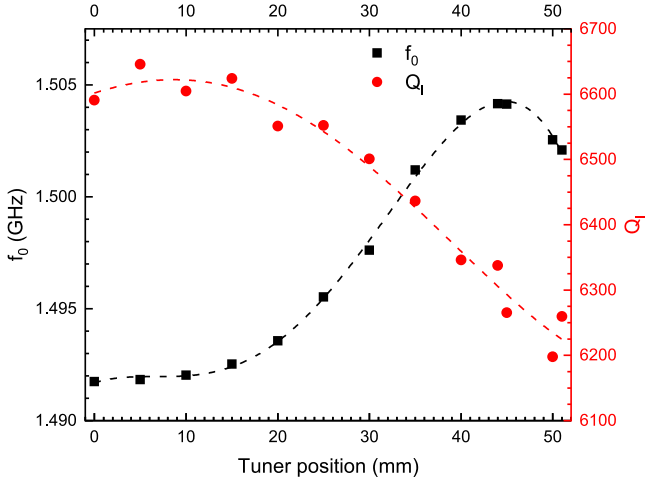

Fig. 6. Measurement of the resonance frequency and loaded quality factor depending on plunger position.

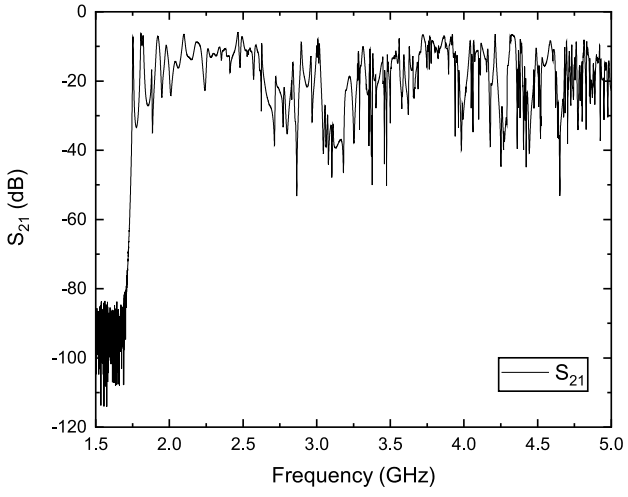

Fig. 7. RF transmission between two transdampers through the cavity body.

as is also the case in the 500 MHz EU HOM-damped cavity, where this arrangement optimizes coupling to the HOMs [16].

- *Coupler reflections and mode splitting:* Because the HOM couplers are not perfectly matched, up to 20% of the extracted HOM power is reflected back into the cavity. As a result, the HOM couplers effectively behave as additional resonators coupled to the cavity body. Consequently, each mode splits into a passband of four coupled modes: three resonances associated with the HOM couplers and one with the cavity body itself. This configuration creates a dense spectrum of modes, most of which are irrelevant to particle dynamics.

These phenomena complicate the specification of both calculated and measured shunt impedances. In particular, transverse shunt impedances can no longer be defined using conventional physical-mathematical methods due to the highly deformed mode geometries. To address this issue, the longitudinal shunt impedances of monopole modes were calculated along the mechanical axis of the cavity, following standard procedures. For dipole modes, the maximum longitudinal shunt impedance was determined around a cylindrical mandrel with a radius of 5 mm centered on the cavity axis to identify their polarization direction. At this azimuthal location, the transverse shunt impedance was subsequently calculated. The same procedure was applied to higher polarizations. The values obtained through these calculations were then used to generate Figs. 8 and 9.

3.4. Bead pull measurements

3.4.1. Basics of bead pull data analysis

When a small object, a bead in this case, perturbs the electromagnetic fields in a cavity, each mode of the frequency f experiences a frequency shift Δf [25], which can be expressed as:

$$\frac{\Delta f}{f} = \frac{\Delta W}{W}, \tag{7}$$

where ΔW is the change of the energy W stored in the mode. The value of ΔW depends on the material and geometry of the bead, with reference values available in the literature for various bead geometries. For example for a metallic spherical bead

$$\Delta W = \pi a^3 \left(-\epsilon_0 E^2 + \frac{\mu_0 B^2}{2} \right), \tag{8}$$

and for a dielectric ball

$$\Delta W = \pi a^3 \left(-\epsilon_0 E^2 \frac{\epsilon - 1}{\epsilon + 1} \right), \tag{9}$$

where a is the bead diameter, E and B are the field amplitudes at the position of the bead, ϵ_0, μ_0 are fundamental constants and ϵ is the bead

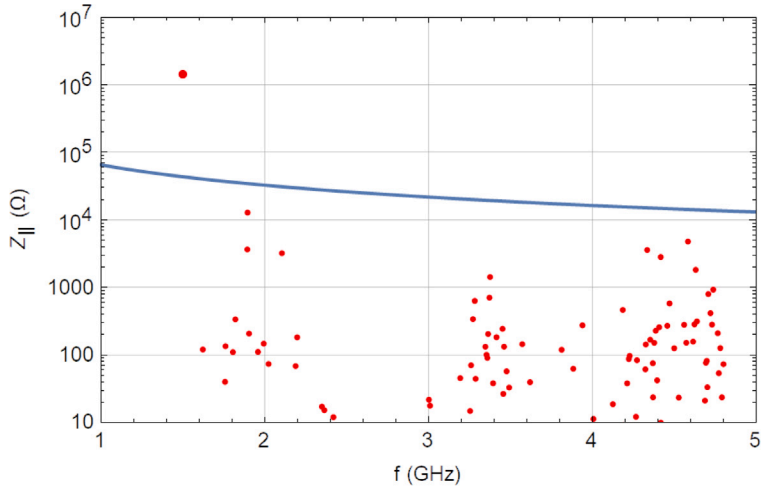

Fig. 8. Longitudinal shunt impedances of one cavity for the first 300 HOMs, including the fundamental mode. The blue curve represents the longitudinal impedance threshold $Z_{\parallel}^{\text{thresh}}$ for BESSY II.

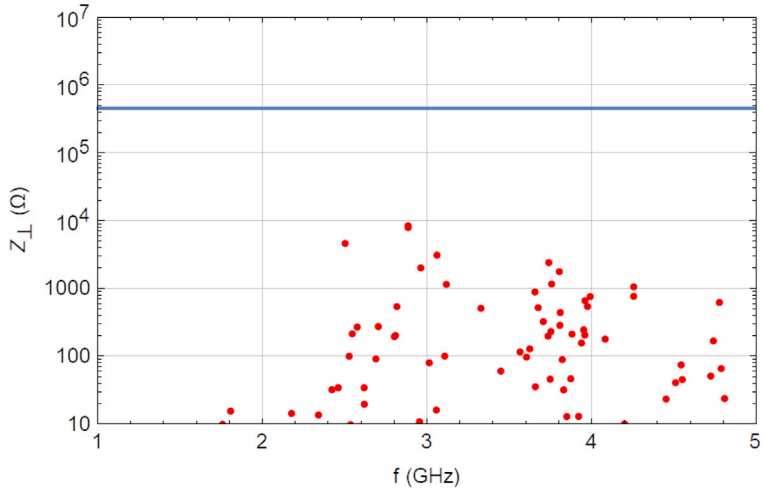

Fig. 9. Transverse shunt impedances of one cavity for the first 299 HOMs. The blue curve represents the transverse impedance threshold $Z_{\perp}^{\text{thresh}}$ for BESSY II.

permittivity.

Typically, a better signal-to-noise ratio in bead pull measurements is achieved if the phase change $\Delta\varphi$ of the mode instead of the frequency shift is measured:

$$\frac{\Delta f}{f} = \frac{\tan \Delta\varphi}{2Q_L} \tag{10}$$

For the fundamental (TM_{010}) mode, the field components can be approximated as $\vec{E} = (0, 0, E_z)$ and $\vec{B} = 0$. Using the definition of the shunt impedance:

$$\frac{R}{Q} = \frac{1}{\omega U}\left|\int E_z exp\left(i\frac{\omega z}{\beta c}\right) dz\right|^2, \tag{11}$$

the final expression for the shunt impedance can be derived as:

$$\left(\frac{R}{Q}\right) Q_L = \frac{1}{4\pi^2 a^3 \epsilon_0 f}\left|\int \sqrt{\tan(\Delta\varphi)} exp\left(i\frac{\omega z}{\beta c}\right) dz\right|^2. \tag{12}$$

For higher-order modes, the field geometry becomes complex, often requiring measurements with multiple beads of different materials and shapes. Simulated results for higher-order modes can be used to predict the expected bead pull signal and validate experimental measurements.

3.4.2. Measurement system

To characterize the cavity modes, an automated bead pull measurement system was developed and constructed at HZB. Details of the system are shown in Fig. 10.

The system consists of two motorized two-coordinate tables to move the bead in the transverse plane and a motorized system to pull the bead longitudinally. A VNA, synchronized with the longitudinal motion of the bead, is used to track the phase variation of the cavity mode at a fixed frequency. The used beads include a metal syringe needle (10 mm × ⌀1.3 mm), a metal sphere (⌀3.3 mm, Pb), and a dielectric sphere (⌀10 mm). A graphical user interface (GUI) was developed to automate the measurements for a predefined set of frequencies on a transverse mesh.

3.4.3. Experimental results

Fundamental mode

Measurements of the fundamental mode confirmed the shunt impedance values predicted by simulations. The measured parameters are summarized in Table 5.

In Fig. 11, the results of the bead pull measurements are shown. The left panel depicts seven phase shift profiles obtained using a small metallic sphere as the bead. The right panel shows the mesh of transverse bead positions for each measurement. Fig. 12 displays a contour plot of the mode impedance overlaid (not to scale) with the

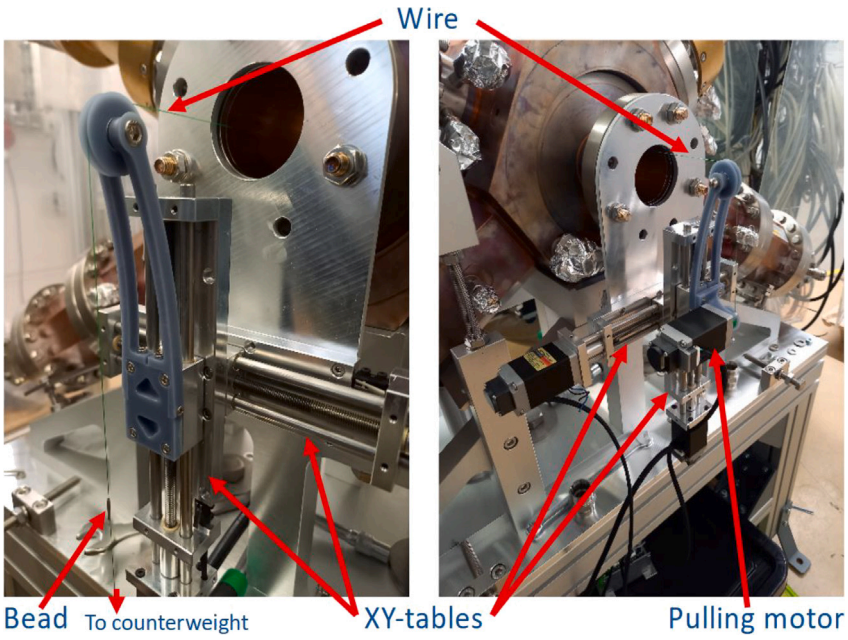

Fig. 10. Bead pull measurement system developed at HZB.

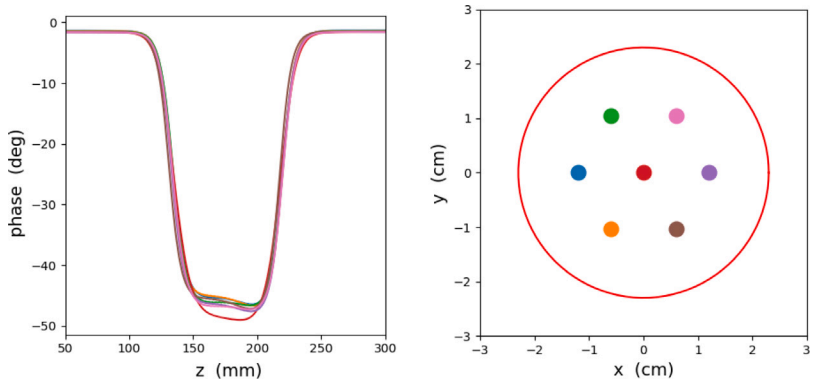

Fig. 11. Left: Bead pull measurements of the fundamental mode at 1.499 GHz using a spherical 3.3 mm bead. Rigth: Mesh of the seven measurements.

Table 5
Fundamental mode parameters obtained with the bead pull technique.

Frequency [GHz]	Shunt impedance [MΩ]	Q_0
1.499	1.05	13 200

cavity geometry, indicating the positions of the plunger and the main coupler. The observed asymmetry in the phase shift profile and the shift of the electromagnetic center of the mode were also predicted by simulations.

Higher order modes (HOMs)

The analysis of HOM measurements is challenging due to the complex mode geometries, where assumptions about field symmetry are not always valid. As previously explained, this complexity is attributed to the asymmetry of the cavity caused by open ports (e.g., the input power coupler, plunger, damping arms, and pick-up loop) and the small volume of the 1.5 GHz cavity. Nevertheless, bead pull measurements allow upper estimates of mode impedances under the assumption $\vec{E} = (0, 0, E_z)$ for a dielectric bead.

For the most critical modes, simulations were used to determine field directions and verify consistency between simulated and measured

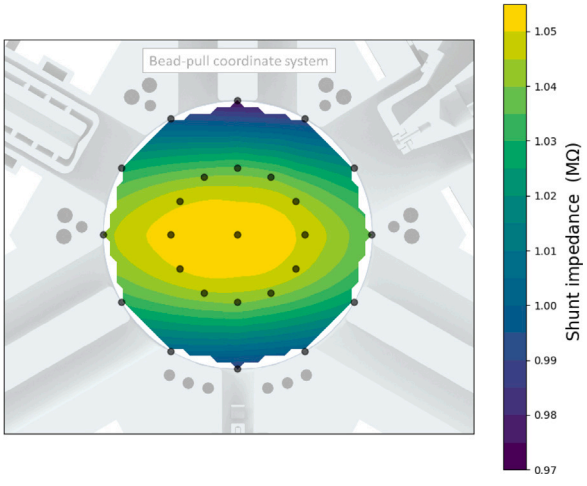

Fig. 12. Fundamental mode: contour plot of the mode R/Q, using data of a spherical 3.3 mm bead.

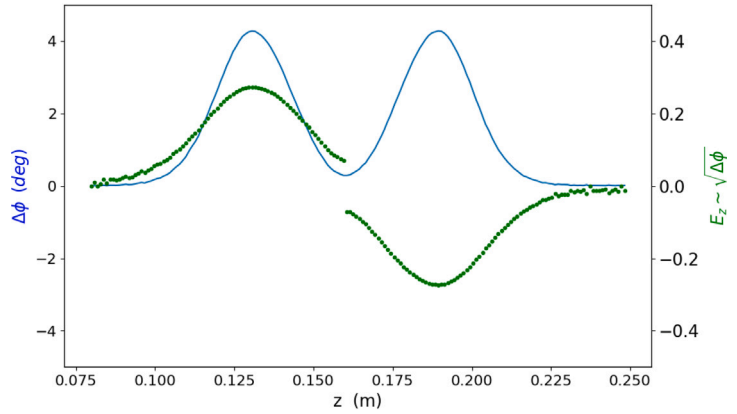

Fig. 13. TM011-like mode at 2.09527 GHz measured with a plastic spherical 10 mm bead.

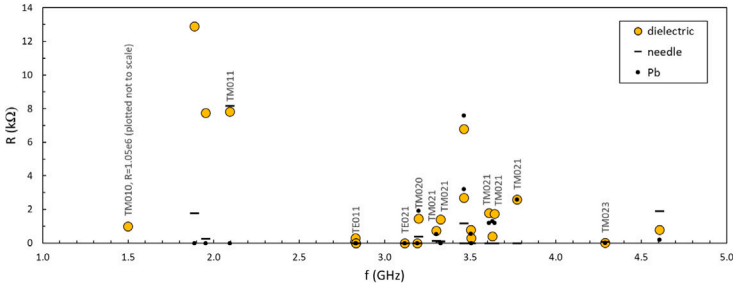

Fig. 14. Loaded shunt impedance of monopole (and unidentified) HOMs. Analysis of the measurements with three beads is presented.

Table 6
TM011 mode parameters obtained with the bead pull technique.

Frequency [GHz]	R/Q [Ω]	Shunt impedance (R) [kΩ]
2.095	45.4	8,17

impedance values. Comparing results from different beads helps refine these estimates. Measurements with the syringe needle bead are particularly sensitive to longitudinal electric fields and provide the closest approximations.

To give an estimation of how accurate measurements for HOMs are, the results for one of the most dangerous monopoles, the mode TM011, are shown in Fig. 13. The blue solid line represents the phase change as a function of the longitudinal coordinate (z), while the green dotted line represents the field profile $E \sim \sqrt{\Delta\varphi}$, assuming E_z changes direction at the cavity center. The observed discontinuity is attributed to the misalignment of the transverse electromagnetic and mechanical centers, causing small transverse field components at the cavity center. Table 6 summarizes the measured parameters for the TM011 mode.

Figs. 14 and 15 summarize the measured impedance of HOMs. If the mode symmetry could be identified, it is indicated above the measurement points. For modes with good signal-to-noise ratios, impedance estimates from all beads are provided.

All beads were calibrated using a copper pillbox cavity with small openings, to ensure the theoretical mode frequencies and field distributions were undisturbed.

3.5. Energy loss of electron bunches traversing the 3rd harmonic cavity

Another important issue addressed in this study was the evaluation of the energy deposited by the bunches traversing the 3rd harmonic cavity across all frequencies, particularly during high-current operation. This analysis is crucial to ensure that the coaxial feedthrough and the matched power load outside the vacuum can handle the maximum HOM power extracted from the beam. To calculate the energy loss, an analytical method developed by R. B. Palmer at SLAC in 1987 [26] was applied. For clarity, several general remarks regarding the physical process of energy loss when a highly relativistic bunch crosses a cavity are provided.

At 3 GeV kinetic energy, the passing bunches are highly relativistic, and their contracted field disks cannot interact with the outer periphery of the cavity. Based on the Pythagorean theorem for velocities [27], the radial propagation velocity of the fields is significantly limited. Consequently, the field perturbations generated during cavity traversal propagate slowly within the field disk. The energy loss of an electron bunch in the cavity is therefore determined primarily by the immediate radial environment surrounding the field disk as it enters the cavity from the beam pipe. Upon re-entering the beam tube after crossing the cavity, the radial propagation of the field disk is sheared off, leaving the residual field energy in the cavity.

The energy loss from the field disk results from the diffraction of its frequency components when the bunch enters the cavity space from the beam tube. According to Babinet's principle [28], half of the diffracted energy is radiated into the shadow region, while the other half is radiated into the beam pipe region of the cavity. The shadow region corresponds to the cavity volume with a radius larger than the beam pipe radius, and the energy diffracted into this region is captured by the HOM waveguides. Using Palmer's analytical approach [26], the HOM power extracted into the HOM dampers is given by:

$$\Delta P_{HOM} = \frac{1}{2}(k(\sigma_s) - k_{acc})\frac{T_0}{N_b} I_b^2, \tag{13}$$

where T_0 is the revolution time, N_b is the total number of circulating bunches and I_b is the beam current. $k(\sigma_s)$ is the loss factor which determines the overall energy loss of a bunch into all modes including the fundamental one:

$$k(\sigma_s) = \frac{1}{4\pi\varepsilon_0 a}\sqrt{\frac{g}{2\sigma_s}}. \tag{14}$$

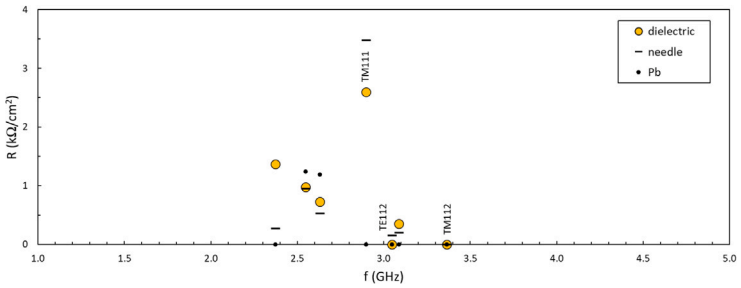

Fig. 15. Loaded shunt impedance of dipole HOMs. Analysis of measurements with three beads is presented.

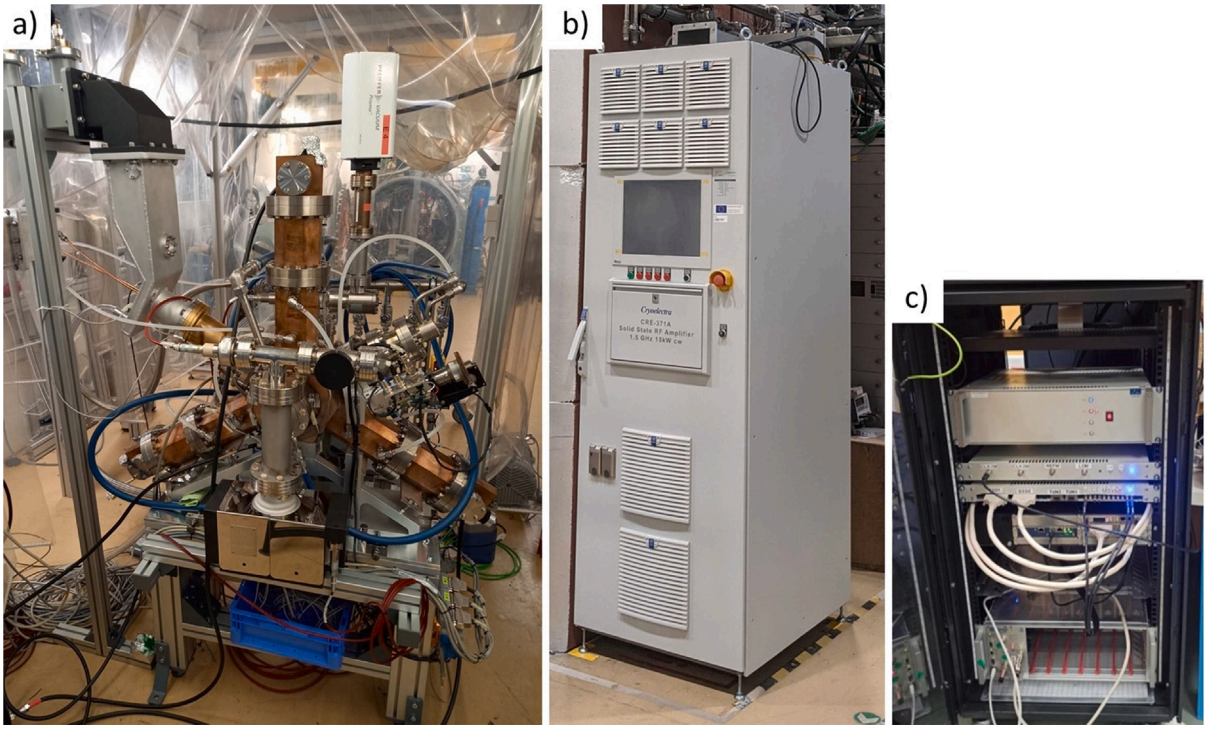

Fig. 16. (a) Cavity installed in HoBiCaT bunker, (b) Solid State Amplifier, (c) LLRF.

This value depends on the beam pipe radius a, the gap length g of the cavity and on the bunch length σ_s. k_{acc} is the loss factor of the fundamental mode and is given by:

$$k_{acc} = \frac{\omega}{2}\left(\frac{R}{Q}\right). \tag{15}$$

Using Eqs. (13), (14), and (15), it was calculated that during normal operation of BESSY II, 300 mA and 400 bunches, a maximum total power loss of 27 W is expected, corresponding to a HOM load of approximately 9 W for each HOM waveguide. This value is well within the specifications of the components. The analytically calculated power loss shows good agreement with CST-MWS simulations, with deviations below 10%.

3.6. High power conditioning

The cavity was installed in the SUPRALAB@HZB testing infrastructure, located in the HoBiCaT bunker, with all necessary infrastructure and safety requirements in place. The experimental setup included the cavity, solid-state amplifier (SSA), waveguides, and digital LLRF, all installed and operational in the lab. For these tests, the β was approximately 0.76.

The pictures in Figs. 16 show the different hardware equipment.

Following the installation of the system, thorough checks of the cooling system, cabling connections, and commissioning of the controls and digital LLRF were carried out. High-power RF conditioning was then initiated. Over a period of two weeks, a combination of pulsed conditioning and continuous power vacuum cleaning was employed. The system achieved a power level of 14 kW (or cavity voltage amplitude of 170 kV), with only a moderate temperature increase observed at critical hot points of the cavity. This confirmed the effectiveness of the cavity's cooling system. Additionally, a vacuum level below 10^{-8} mbar was reached, as shown in Fig. 17.

The results of the laboratory tests demonstrate that the cavity meets all expected performance requirements, including fundamental shunt impedance, HOM damping, and power-handling capability.

4. Tests with beam

Following the successful laboratory testing, the cavity was installed in the BESSY II storage ring. Fig. 18 shows the cavity in its operational position within the tunnel.

Extensive tests were conducted to evaluate the performance of the cavity. These included verifying the HOM damping mechanism and

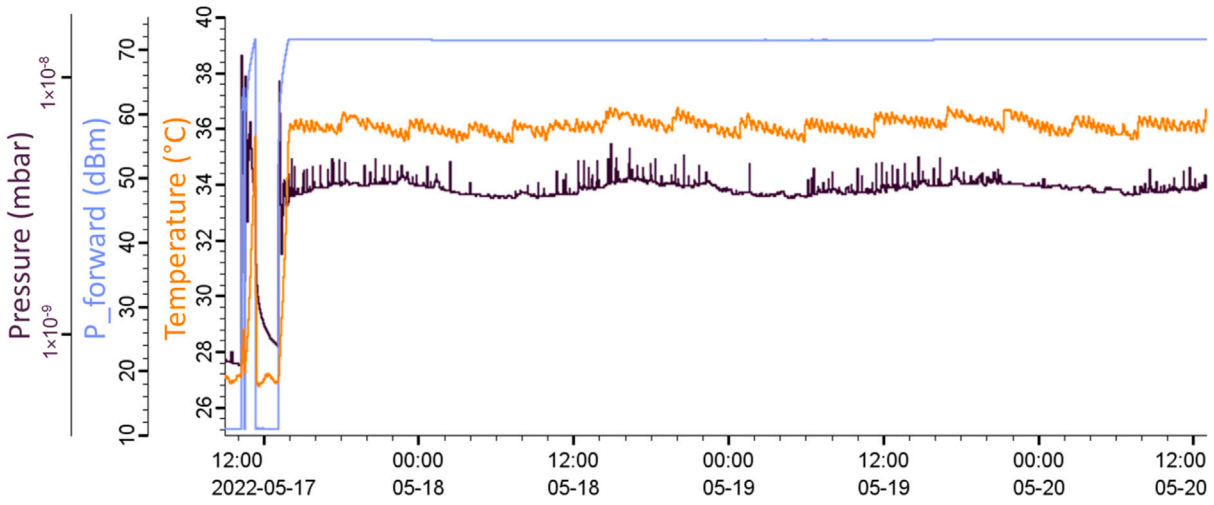

Fig. 17. High power tests in HoBiCaT. Vacuum level (in mbar, log scale), forward power (in dBm), and temperature (in °C at the coupler flange) at 12.5 kW continuous wave (CW) power over approximately three days of operation.

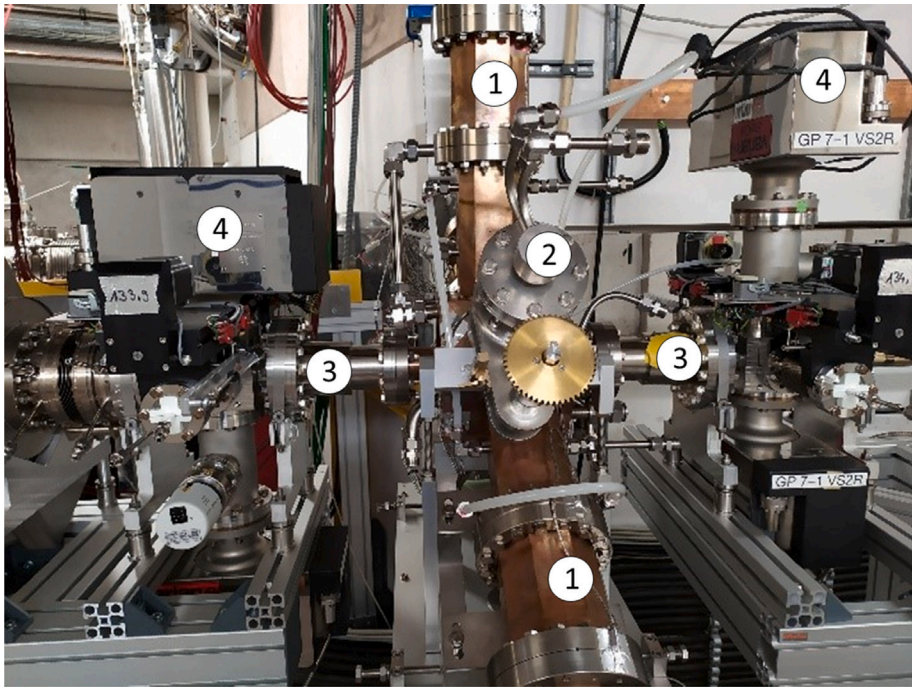

Fig. 18. 3rd harmonic cavity installed in the BESSY II storage ring. (1) Transdampers, (2) plunger, (3) beam pipe, (4) ion getter pumps.

analyzing the bunch lengthening effects in both single-bunch and multi-bunch operation modes. Additionally, lifetime measurements were performed to validate the ultimate goal of the third harmonic system. During all tests, the cavity's coupling factor was set to 0.8, a value which minimizes the reflected power for the specific operational conditions under study.

4.1. HOM measurements

To verify the previous computations on the damping effect of the transdampers on the HOMs shown in Section 3.3, the cavity was excited with a 1 mA single-bunch beam. The spectrum from the pick-up antenna was recorded under two conditions: with the transdampers terminated with 50 Ω, and with an open circuit. In the open-circuit configuration, the power absorbed by the damper arms is reflected back into the cavity body, thereby negating the damping effect. To isolate the single-bunch spectrum from the cavity body, the envelope formed by the peak amplitudes at each revolution frequency was extracted. This process is illustrated in Fig. 19.

The detected peaks were matched between the two measurements. As shown in Fig. 20, the transdampers effectively remove or significantly attenuate all modes below 3 GHz while leaving the fundamental mode unaffected. Above 3 GHz, most modes are attenuated to a lesser extent. However, according to simulations, better damping performance was expected in this frequency range, as indicated in Fig. 4. Further investigations are ongoing to understand the transdampers' response at higher frequencies, even though the measured modes above 3 GHz have shown no observable effects on the beam.

4.2. Single bunch

Since only one harmonic cavity has been installed in the BESSY II storage ring, the main RF cavity voltage was set to 400 kV to

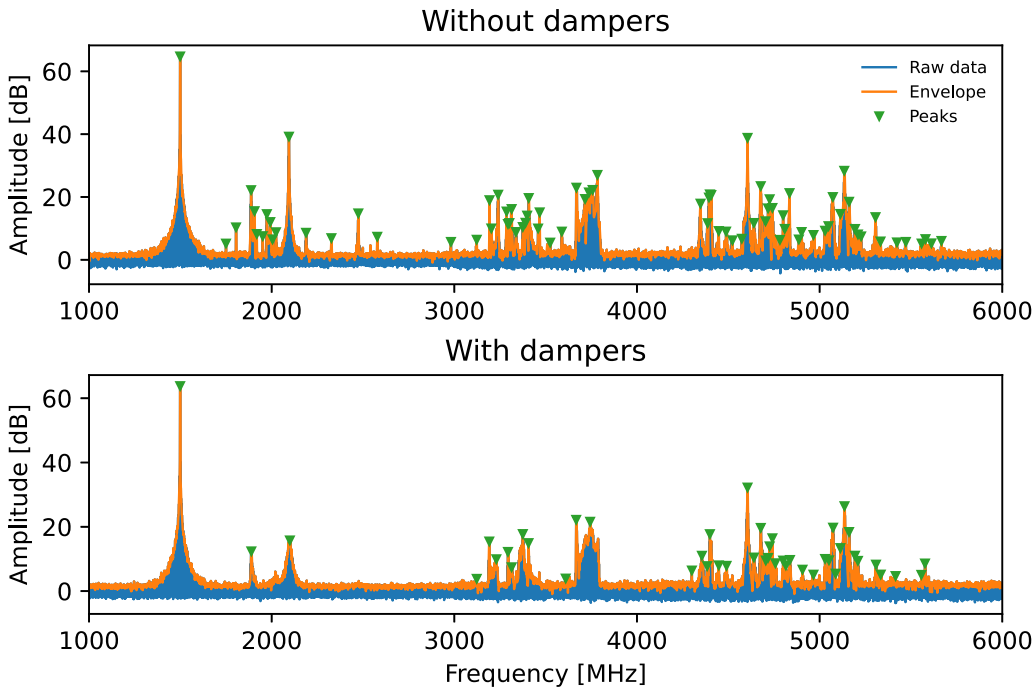

Fig. 19. Full single bunch spectrum.

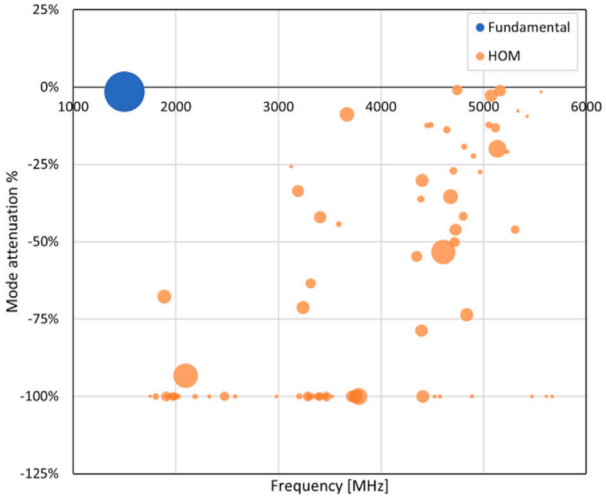

Fig. 20. Attenuation of individual peaks in %. Bubble radius is proportional to mode amplitude without dampers in dB.

ensure that the harmonic cavity could operate at its optimal setting for achieving a flat potential. This configuration required the harmonic cavity voltage to be set at 108 kV.

We measured the single-bunch charge distribution using a high-resolution streak camera (see Fig. 21), while maintaining a beam current of approximately 0.5 mA to minimize the effects of short-range wakefields from the ring. To effectively probe the longitudinal focusing force, we recorded the longitudinal oscillation frequency of the bunch using the BBFB (bunch-by-bunch feedback) system. The harmonic voltage was varied from 10 kV to a maximum of 130 kV in increments of 5 kV. ϕ_h was set to the value that meets the flat potential condition, determined by performing a phase scan from −180° to 180° and selecting the value that minimized f_s.

The variations observed in the measured bunch charge distributions (illustrated in Fig. 22) can be attributed primarily to the progressive transformation of the corresponding potential wells, defined by the RF system, from a quadratic to a quartic form.

Qualitatively, the bunch distribution can be expressed as:

$$\rho(s) = Ae^{-U(s)/U_c} \tag{16}$$

where A represents a normalization constant,

$$U_c = \alpha^2\sigma_E^2 c/2 \tag{17}$$

with α being the momentum compaction factor, σ_E the relative energy spread and $U(s)$ denotes the potential well. We conducted a fitting process, employing a potential well model defined as:

$$U(s) = a_1 s + a_2 s^2 + a_3 s^3 + a_4 s^4 + a_5 s^5 \tag{18}$$

which is determined by the RF voltages and phases in both the main and harmonic cavities [19]. This model effectively captures the observed bunch distributions, as demonstrated in Fig. 22.

Using the fitted coefficients a_i of the potential well, the linear synchrotron frequency can be determined as $\sqrt{2a_2 c}$, expressed in radians per second [19]. This concept is valid only when the potential well is primarily governed by the quadratic term (s^2), as the motion becomes increasingly nonlinear when the quartic term (s^4) starts to dominate. The computed synchrotron frequencies were compared with the measured values, as shown in Fig. 23.

The remarkable agreement between the modeled and measured synchrotron frequencies (f_s) serves two critical purposes. First, it confirms the validity and accuracy of the fitting model. Second, it demonstrates that linear motion effectively describes bunch dynamics when the potential well remains predominantly quadratic. Discrepancies between the model and measurements are generally below 100 Hz. However, as the potential well transitions to a quartic shape, the spread of f_s increases, resulting in a broader distribution (approximately 0.5 kHz rms under the optimal potential condition). Beyond this regime, the formation of two distinct potential wells (as indicated by the presence of two humps in the bunch charge distribution) introduces uncertainty about which well or combination of wells contributes to the measured frequency.

In summary, the agreement between the model and single-bunch measurements is excellent. Under the specified conditions, the bunch length was increased by a factor of 3 compared to the initial zero-current bunch length of 8.6 mm. This significant bunch lengthening at

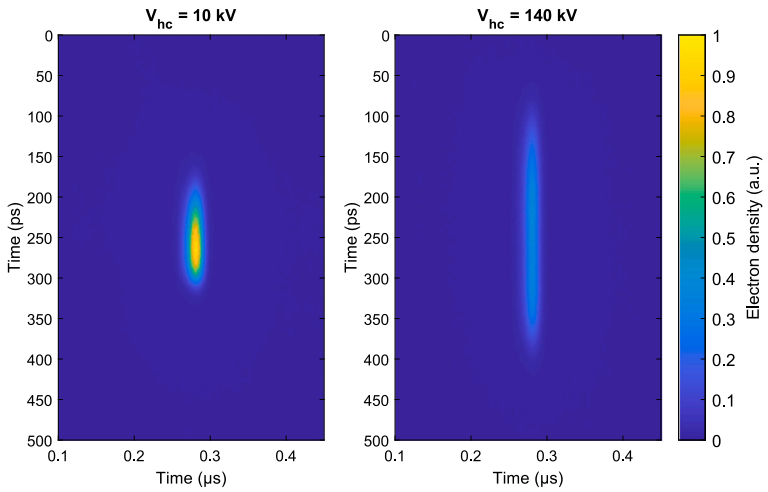

Fig. 21. Streak camera images for the single bunch mode, showing the bunch lengthening effect of the harmonic cavity.

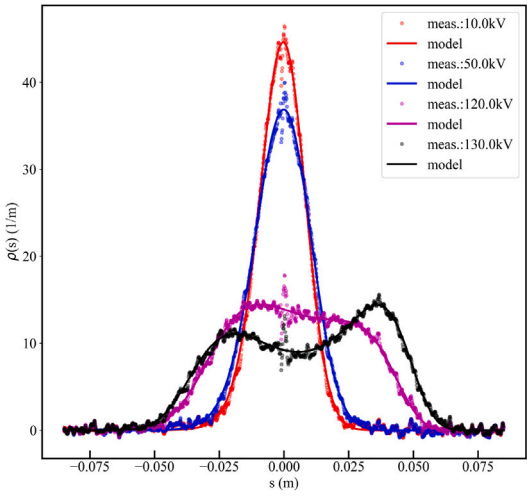

Fig. 22. Single low current bunch measured charge distribution at harmonic voltage settings 10, 50, 120, 130 kV (with streak camera), and the corresponding fitting to a model (solid lines).

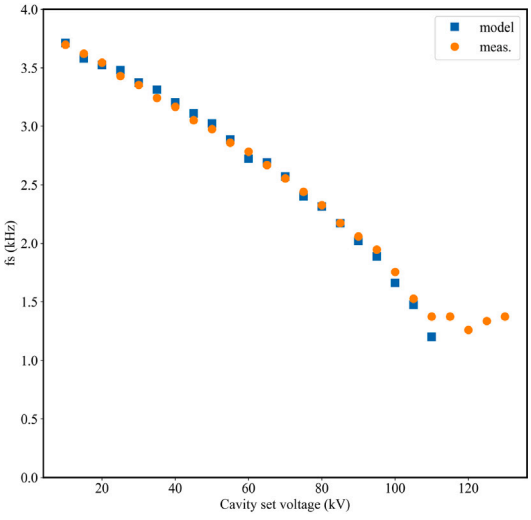

Fig. 23. Measured and calculated synchrotron frequencies (f_s) as a function of harmonic cavity voltage. The last computed data point corresponds to 110 kV.

such a low current underscores the advantage of the cavity being active, enabling optimal lengthening across the entire beam current range.

4.3. Homogeneous filling pattern

The next step was to inject a multibunch homogeneous filling pattern, with all the RF buckets filled, and check the performance of the 3rd harmonic cavity.

Fig. 24 shows the streak camera images showing the bunch lengthening of all the bunches, quite homogeneously, at three different harmonic voltages, for a 12 mA beam.

The fact that we have only installed one harmonic cavity in the storage ring makes it difficult to test the full capability of the harmonic system at full current, i.e 300 mA. Several strategies were used in order to reach the harmonic voltage that meets flat potential condition with a high current homogeneous filling pattern.

First, 300 mA of current in homogeneous filling were injected in the storage ring with the harmonic voltage at 130 kV and the fundamental voltage at 800 kV, using only two main cavities instead of the usual four needed for operation. Then, the main voltage was gradually reduced targeting a total of 460 kV, the value which would achieve flat potential. At 615 kV of main voltage, the measured bunch length was 140 ps of FWHM. ϕ_h was set to 0°, which we refer to as zero-crossing, in all cases. Even though this phase value will never meet the flat potential condition, setting the system in a near flat potential state, this was done for the sake of increasing the system stability.

However, after reducing the main RF voltage to approach the target voltage for a flat potential, large coherent longitudinal oscillations of the beam were observed, ultimately leading to beam loss. This behavior was attributed to a DC Robinson instability, triggered by the combination of low main RF voltage and a limited number of harmonic cavities. To mitigate the observed oscillations, a negative detuning of the main cavities was applied, enabling operation at 615 kV. This result aligned well with theoretical expectations: further detuning reduces the imaginary part of the cavity impedance and suppresses the coherent frequency shift, thereby mitigating the DC Robinson instability [29, 30]. The maximum applied detuning was −30° to prevent excessive reflected power from the cavity.

The second strategy was to set up two main RF cavities at total voltage of 460 kV, while keeping the harmonic one at 130 kV, and inject current progressively. By doing so, it was possible to reach 60 mA in uniform filling pattern in flat potential conditions, i.e. $\xi = 1.0$. The maximum current and flat potential conditions achieved are summarized in Table 7.

A phasor diagram showing how the generator power compensates the beam loading during this second studied case is shown in Fig. 25. In this case, most part of the cavity voltage is driven by the generator.

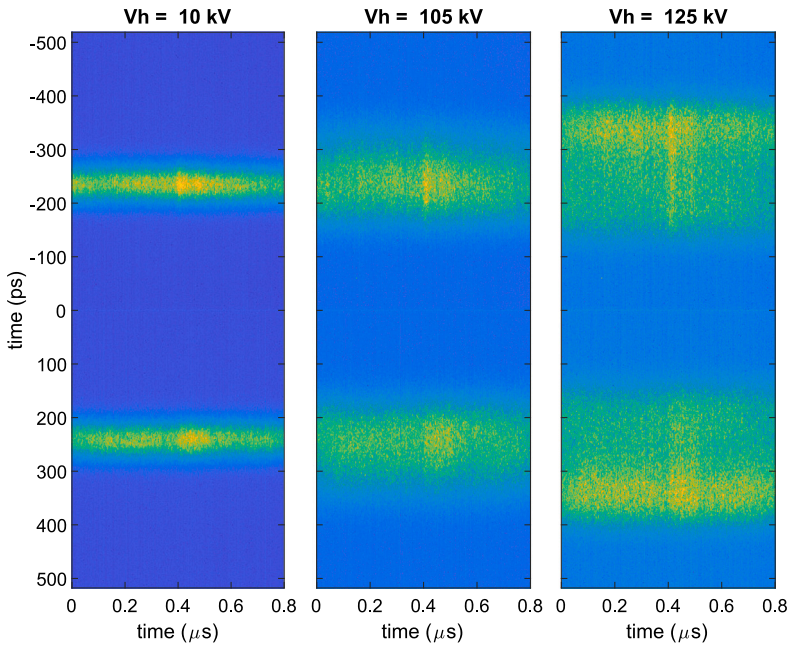

Fig. 24. Streak camera images for homogeneous filling pattern at 12 mA, 400 kV of main RF Voltage and 10 kV (left), 105 kV (center) and 125 kV (right) of harmonic voltage.

Table 7
Homogeneous filling pattern tests summary. These cases are the operation limits found for $\xi = 1.0$ and the nominal 300 mA, respectively.

Current [mA]	Main voltage [kV]	Harmonic voltage [kV]	ξ
60	460	130	1.0
300	615	130	0.7

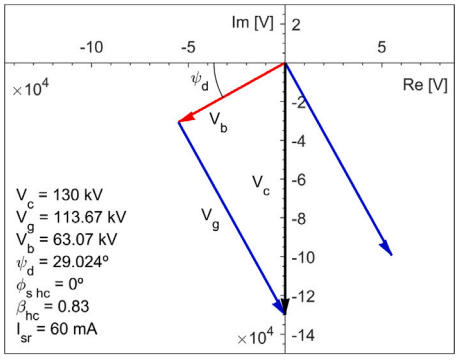

Fig. 25. HC phasor plot for the $\xi = 0.98$ case, showing how the beam loading is compensated with the generator power.

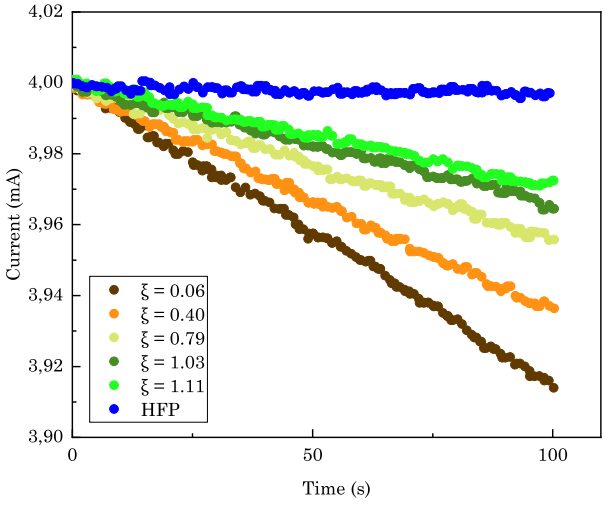

Fig. 26. Current trends for homogeneous uniform filling (HFP), and for single bunch at different harmonic voltages values, expressed as the ratio ξ.

4.4. Beam lifetime

Finally, in order to further confirm the bunch lengthening, the lifetime was also measured for a single bunch. For that, a current of 4 mA was stored and its decay with time was recorded for different values of the harmonic voltage. The main RF voltage has been kept constant to 450 kV so that flat potential can be reached with an harmonic voltage of 126 kV, according to Eqs. (3) and (2).

To distinguish the Touschek effect, the same 4 mA current have been stored spreading them over all the bunches in a homogeneous filling pattern so that we can evaluate the lifetime component due to gas scattering. Fig. 26 shows the current trends for these cases for different ξ values.

The lifetime has been measured by fitting the data from Fig. 26 to:

$$\frac{1}{\tau} = -\frac{1}{I_0}\frac{\Delta I}{\Delta t} \tag{19}$$

where $I_0 = 4.0$ mA.

For the HFP the fitted lifetime is $\tau = 58.8 \pm 5.2$ h, and we use this value to subtract the gas scattering lifetime component from the fitted lifetime in single bunch, and so, estimate the Touschek component.

Fig. 27 summarizes the Touschek lifetime fittings for every ξ. The gain factor for the Touschek lifetime, calculated as the ratio between the lifetime fittings of the trends with respect the one at $\xi = 0$, is also shown.

It is worth noting that the increase of the Touschek lifetime at the quartic potential is around a factor of 3, fitting remarkably with the bunch lengthening factor obtained in the previous paragraph.

5. Conclusions

We have developed a full active harmonic RF system, including the cavity, the amplifier and the LLRF systems, working at 1.5 GHz. We have successfully tested the system in the lab, and with beam at the

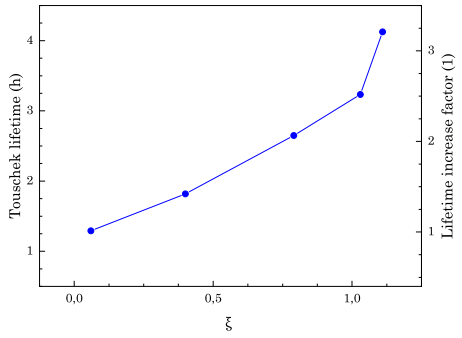

Fig. 27. Touschek lifetime and gain factor as a function of ξ.

BESSY II storage ring.

We have demonstrated the full capacity of the active harmonic RF system for operating at any beam current condition, from low current single bunch up to high current multibunch.

We have properly modeled the double RF system, and we are confident the system will perform as expected for the BESSY II ring as well as for ALBA, and the upgraded ALBA II storage rings.

Though the results of HOM simulations presented in Section 3.3 and measured values presented in Sections 3.4 and 4.1 are in good agreement for the cavity fundamental mode and HOMs up to ~3 GHz, there are significant differences at higher frequencies. In future versions of the cavity, a revision of the transdampers' construction is foreseen to improve the RF transmission at higher frequencies.

Still remaining to investigate is the behavior of the system when a gap is introduced in the beam filling pattern, which will lead to transient beam loading effects, and reduce the bunch lengthening efficiency.

CRediT authorship contribution statement

F. Perez: Writing – review & editing, Supervision, Project administration, Funding acquisition. **J. Alvarez:** Formal analysis. **I. Bellafont:** Methodology, Investigation. **B. Bravo:** Methodology. **J. Ocampo:** Data curation, software simulation. **A. Salom:** Conceptualization. **P. Solans:** Writing – original draft, Methodology, Investigation. **M. Ebert:** Conceptualization. **N.-O. Fröhlich:** Resources. **P. Hülsmann:** Software simulations, Investigation. **R. Onken:** Resources, Project administration. **W. Anders:** Project administration. **V. Duerr:** Formal analysis. **T. Löwner:** Resources. **A. Matveenko:** Methodology, Investigation. **M. Ries:** Project administration. **L. Shi:** Software simulations. **Y. Tamashevich:** Resources. **A. Tsakanian:** Software simulations. **H. De Gersem:** Software simulations. **W. Müller:** Software simulations, Investigation.

Declaration of competing interest

The authors declare that they have no known competing financial interests or personal relationships that could have appeared to influence the work reported in this paper.

Acknowledgments

We acknowledge the help of many colleagues and technicians from ALBA, HZB and DESY which have make this work possible. The cavity prototype design and construction were co-funded by the European Regional Development Fund (ERDF) within the Framework of the Smart Growth Operative Programme 2014–2020. This work has been performed under the Collaboration Agreement RCN-CIN202100124, Spanish BOE Resolution 8506 of May 14th, 2021, published in May 21st, 2021.

Data availability

Data will be made available on request.

References

[1] F. Pérez, et al., ALBA II acelerator upgrade project, JACoW IPAC2022 (2022) TUPOMS027, http://dx.doi.org/10.18429/JACoW-IPAC2022-TUPOMS027.

[2] A. Loulergue, et al., TDR baseline lattice for the upgrade of SOLEIL, in: Proc. 13th International Particle Accelerator Conference, IPAC'22, 2022, pp. 1393–1396.

[3] A. Streun, SLS 2.0, the upgrade of the swiss light source, in: Proc. IPAC'22, JACoW Publishing, Geneva, Switzerland, 2022, pp. 925–928.

[4] P. Goslawski, et al., BESSY III status report and lattice design process, in: Proc. IPAC'22, 2022, pp. 1417–1419.

[5] I. Agapov, et al., PETRA IV storage ring design, in: Proc. IPAC'22, 2022, pp. 1431–1434.

[6] E. Karantzoulis, A. Fabris, S. Krecic, The elettra 2.0 project, in: Proc. IPAC'22, 2022, pp. 1459–1462.

[7] I. Martin, et al., Diamond-II storage ring developments and performance studies, in: Proc. IPAC'22, 2022, pp. 1491–1494.

[8] G. R.Biscardi, RF system for bunch lengthening, JACoW IPAC1995 (1995) WPP03.

[9] r. Andersson, et al., The 100 MHz RF system for the MAX IV storage rings, Conf. Proc. C 110904 (2011) 193–195.

[10] J.M. Byrd, K. Baptiste, S. De Santis, S. Kosta, C.C. Lo, D. Plate, R.A. Rimmer, M. Franks, Design of a higher harmonic RF system for the advanced light source, Nucl. Instrum. Methods A 439 (2000) 15–25, http://dx.doi.org/10.1016/S0168-9002(99)00892-X.

[11] W. Anders, P. Kuske, HOM damped NC passive harmonic cavities at BESSY, Conf. Proc. C 030512 (2003) 1186.

[12] M. Pedrozzi, et al., First operational results of the 3rd harmonic super conducting cavities in SLS and ELETTRA, Conf. Proc. C 030512 (2003) 878.

[13] N. Yamamoto, A. Gamelin, P. Marchand, R. Nagaoka, T. Yamaguchi, Stability survey of a double RF system with RF feedback loops for bunch lengthening in a low-emittance synchrotron ring, in: Proc. IPAC'23, in: IPAC'23 - 14th International Particle Accelerator Conference, number 14, JACoW Publishing, Geneva, Switzerland, 2023, pp. 3498–3501, http://dx.doi.org/10.18429/JACoW-IPAC2023-WEPL161, URL: https://indico.jacow.org/event/41/contributions/2061.

[14] N. Yamamoto, T. Takahashi, S. Sakanaka, Reduction and compensation of the transient beam loading effect in a double RF system of synchrotron light sources, Phys. Rev. Accel. Beamsv. 21 (2018) 012001, http://dx.doi.org/10.1103/PhysRevAccelBeams.21.012001, URL: https://link.aps.org/doi/10.1103/PhysRevAccelBeams.21.012001.

[15] A. Salom, J. Alvarez, B. Bravo, F. Pérez, HOM damped normal conducting 1.5 GHz cavity design evolution for the 3rd harmonic system of the ALBA storage ring, in: 10th International Particle Accelerator Conference, 2019, WEPRB060, http://dx.doi.org/10.18429/JACoW-IPAC2019-WEPRB060.

[16] E. Weihreter, Status of the European HOM damped normal conducting cavity, in: Proc. EPAC'08, in: European Particle Accelerator Conference, number 11, JACoW Publishing, Geneva, Switzerland, 2008, pp. 2932–2936, URL: https://jacow.org/e08/papers/THXM03.pdf.

[17] B. Bravo, J. Alvarez, F. Pérez, A. Salom, 1.5 GHz cavity design for the CLIC damping ring and as active third harmonic cavity for ALBA, in: Proc. of International Particle Accelerator Conference (IPAC'17), Copenhagen, Denmark, 14-19 May, 2017, in: International Particle Accelerator Conference, number 8, JACoW, Geneva, Switzerland, 2017, pp. 4263–4265, http://dx.doi.org/10.18429/JACoW-IPAC2017-THPIK078, URL: http://jacow.org/ipac2017/papers/thpik078.pdf.

[18] J.M. Byrd, M. Georgsson, Lifetime increase using passive harmonic cavities in synchrotron light sources, Phys. Rev. ST Accel. Beamsv. 4 (2001) 030701, http://dx.doi.org/10.1103/PhysRevSTAB.4.030701, URL: https://link.aps.org/doi/10.1103/PhysRevSTAB.4.030701.

[19] R.A. Bosch, K.J. Kleman, J.J. Bisognano, Robinson instabilities with a higher-harmonic cavity, Phys. Rev. ST Accel. Beamsv. 4 (2001) 074401, http://dx.doi.org/10.1103/PhysRevSTAB.4.074401, URL: https://link.aps.org/doi/10.1103/PhysRevSTAB.4.074401.

[20] A. Gamelin, W. Foosang, P. Marchand, R. Nagaoka, N. Yamamoto, Beam dynamics with a superconducting harmonic cavity for the SOLEIL upgrade, JACoW IPAC2022 (2022) WEPOMS003, http://dx.doi.org/10.18429/JACoW-IPAC2022-WEPOMS003.

[21] I. Bellafont, F. Perez, P. Solans, Longitudinal beam dynamics studies with a third harmonic RF system for ALBA-II, JACoW IPAC2023 (2023) WEPL179, http://dx.doi.org/10.18429/JACoW-IPAC2023-WEPL179.

[22] J. Ocampo, J. Alvarez, B. Bravo, F. Pérez, A. Salom, P. Solans, Prototype fabrication of an active normal conducting third harmonic cavity for the ALBA storage ring, JACoW IPAC2022 (2022) TUPOMS051, http://dx.doi.org/10.18429/JACoW-IPAC2022-TUPOMS051.

[23] A. Salom, J. Alvarez, B. Bravo, F. Pérez, HOM damped normal conducting 1.5 GHz cavity design evolution for the 3rd harmonic system of the ALBA storage ring, in: Proc. 10th International Particle Accelerator Conference (IPAC'19), Melbourne, Australia, 19-24 May 2019, in: International Particle Accelerator Conference, number 10, JACoW Publishing, Geneva, Switzerland, 2019, pp. 2948–2951, http://dx.doi.org/10.18429/JACoW-IPAC2019-WEPRB060, URL: http://jacow.org/ipac2019/papers/weprb060.pdf.

[24] D. Systèmes, Dassault systèmes acquires realistic simulation software firm - managing automation, 2012, (Archived from the original on 2013-01-28), (Retrieved 07 July 2012).

[25] T. Jurgens, Equations for Bead Pull Cavity Measurements LU-159, Fermilab-LU-159, 1990.

[26] R.B. Palmer, A qualitative study of wake fields for very short bunches, in: S. Chattopadhyay (Ed.), Part. Accel. 25 (1990) 97–106.

[27] H. Goenner, Spezielle relativitätstheorie und die klassische feldtheorie, in: Spezielle Relativitätstheorie und die klassische Feldtheorie / Hubert Goenner, Spektrum Akademischer Verlag, Heidelberg (Germany), 2004, p. XIII 305, ISBN 3-8274-1434-2 2004.

[28] J. Jackson, Classical Electrodynamics, Chapter 9.11, 1975.

[29] S.R. Koscielniak, Robinson-type stability criteria for beam and RF cavity with delayed, voltage-proportional feedback, Part. Accel. 62 (1999) 179–214, URL: https://cds.cern.ch/record/1120318.

[30] J. Jacob, Passive vs active systems, DC Robinson, DLLRF, in: Harmon-LIP Workshop, 2022, URL: https://indico.maxiv.lu.se/event/5098/contributions/6759.